AFRL-RV-PS-
TR-2014-0143

DATA ASSOCIATION USING A MINIMUM-FUEL METRIC

Andris D. Jaunzemis and Marcus J. Holzinger

Georgia Tech Research Corporation
505 10th ST NW
Atlanta, GA 30332-0001

26 Aug 2014

Final Report

AIR FORCE RESEARCH LABORATORY
Space Vehicles Directorate
3550 Aberdeen Ave SE
AIR FORCE MATERIEL COMMAND
KIRTLAND AIR FORCE BASE, NM 87117-5776

DTIC COPY
NOTICE AND SIGNATURE PAGE

This report is the result of contracted fundamental research deemed exempt from public affairs security and policy review in accordance with SAF/AQR memorandum dated 10 Dec 08 and AFRL/CA policy clarification memorandum dated 16 Jan 09. This report is available to the general public, including foreign nationals. Copies may be obtained from the Defense Technical Information Center (DTIC) (http://www.dtic.mil).

AFRL-RV-PS-TR-2014-0143 HAS BEEN REVIEWED AND IS APPROVED FOR PUBLICATION IN ACCORDANCE WITH ASSIGNED DISTRIBUTION STATEMENT.

//SIGNED//
MORGAN BALDWIN
Program Manager

//SIGNED//
PAUL HAUSGEN
Technical Advisor, Spacecraft Component Technology Branch

//SIGNED//
BENJAMIN M. COOK, Lt Col, USAF
Deputy Chief, Spacecraft Technology Division
Space Vehicles Directorate

REPORT DOCUMENTATION PAGE

Form Approved
OMB No. 0704-0188

1. REPORT DATE *(DD-MM-YYYY)*	**2. REPORT TYPE**	**3. DATES COVERED** *(From - To)*
26-08-2014	Final Report	26 Apr 2013 – 21 Jul 2014

4. TITLE AND SUBTITLE
Data Association Using a Minimum-Fuel Metric

5a. CONTRACT NUMBER
FA9453-13-1-0282

5b. GRANT NUMBER

5c. PROGRAM ELEMENT NUMBER
63401F

6. AUTHOR(S)
Andris D. Jaunzemis and Marcus J. Holzinger

5d. PROJECT NUMBER
5083

5e. TASK NUMBER
PPM00015595

5f. WORK UNIT NUMBER
EF010975

7. PERFORMING ORGANIZATION NAME(S) AND ADDRESS(ES)
Georgia Tech Research Corporation
505 10th ST NW
Atlanta, GA 30332-0001

8. PERFORMING ORGANIZATION REPORT NUMBER

9. SPONSORING / MONITORING AGENCY NAME(S) AND ADDRESS(ES)
Air Force Research Laboratory
Space Vehicles Directorate
3550 Aberdeen Ave. SE
Kirtland AFB, NM 87117-5776

10. SPONSOR/MONITOR'S ACRONYM(S)
AFRL/RVSV

11. SPONSOR/MONITOR'S REPORT NUMBER(S)
AFRL-RV-PS-TR-2014-0143

12. DISTRIBUTION / AVAILABILITY STATEMENT
Approved for public release; distribution is unlimited.

13. SUPPLEMENTARY NOTES

14. ABSTRACT

Data association for Uncorrelated Tracks (UCTs) is a persistent and difficult problem in Space Situational Awareness. Space objects (SOs) often maneuver or are perturbed between observations, and when new measurements are collected, these new UCTs not always easily correlated with existing catalog objects. Presently, orbit element gating, Euclidean distances, and Mahalanobis distances are considered in the literature as tools with which UCTs may be appropriately associated. This Final Report details the software structure and implementation of a UCT association approach that examines the control effort (e.g., fuel) required for the newly observed SO to correspond to a previously observed SO. Synthetic data and on-orbit Wide Area Augmentation System (WAAS) data are both used to test the utility of the control distance data association approach. This Final Report details a) the contract statement of work, b) the software framework and implementation, c) a brief summary of the theory, d) a description of the synthetic and on-orbit WAAS data scenarios, e) comparison and analysis of several association metrics, and f) extensions to the control distance theory.

15. SUBJECT TERMS Validate Fuel Distance Approach; Uncorrelated Tracks; UCTs; Theory Development; Test Scenario Design; Space Situational Awareness; SSA; Resident Space Object; RSO; Real-Time Track Correlation; Geostationary Earth Orbit; GEO

16. SECURITY CLASSIFICATION OF:			**17. LIMITATION OF ABSTRACT**	**18. NUMBER OF PAGES**	**19a. NAME OF RESPONSIBLE PERSON**
a. REPORT	**b. ABSTRACT**	**c. THIS PAGE**			Morgan Baldwin
Unclassified	Unclassified	Unclassified	Unlimited	36	**19b. TELEPHONE NUMBER** *(include area code)* (505) 846-9600

(This page intentionally left blank)

TABLE OF CONTENTS

Section **Page**

LIST OF FIGURES

Figure **Page**

1.0 SUMMARY

In this study, the tasks of correlating observations and detecting maneuvers of space objects are addressed through application of minimum-fuel distance metrics, which provide a natural tool with which to associate space object observation data. A numerical trajectory optimization software is developed to solve deterministic minimum-fuel boundary value problems, specifically for impulsive and low-thrust trajectories. A framework, referred to as the Data Association using Minimum-Fuel Maneuver Metric (DAMMM) algorithm, is implemented to utilize the trajectory optimization software and control distance metrics for maneuver hypothesis testing, incorporating existing theory accounting for boundary condition uncertainty. A more detailed explanation of this algorithm and the components therein can be found in Appendix A. A simulated, realistic scenario is constructed to test the algorithm, and the results are compared to real data from a similar scenario gathered from Wide Area Augmentation System (WAAS) data. Using the simulated and operational data results, the algorithm is tested to evaluate its limitations and tuned for application to operational use. The control distance metric data association technique is compared to other data association techniques (e.g. Euclidean and Mahalonobis distances), revealing the merits of the control distance metric in orbital mechanics applications.

2.0 INTRODUCTION

The problem of properly correlating on-orbit observations and detecting object maneuvers is a challenging and persistent endeavor. There are currently at least 17,000 trackable on-orbit objects, 1,000 of which are active [1, 2], and these numbers are expected to grow significantly due to improved tracking capabilities, new launches, and continued debris generation [3]. Predicting conjunction events is a difficult task [4]; however, recent events highlight the mutual interest that national and private operators share for accurate object correlation and maneuver detection capability [5].

The objective of this study is to validate a novel method for correlating space object tracks with known Resident Space Objects (RSOs) and to characterize and reconstruct RSO maneuvers in support of the Space Situational Awareness (SSA) Mission Area. The problem of correlating Uncorrelated Tracks (UCTs) over large time periods is particularly difficult when objects maneuver during observation gaps. Even relatively small station-keeping maneuvers at Geostationary Earth Orbit (GEO) can result in position discrepancies of many kilometers after an observation gap. UCT correlation is further confounded by state estimate uncertainties. Since both the initial and final UCTs are best estimates, with associated uncertainty distributions, the question of correlation becomes difficult to answer in operational settings, particularly in densely-populated regions of the space environment.

Given a propagated best estimate of the state and its associated distribution, correlating UCTs tests the hypothesis that a newly observed state (with its associated distribution) could possibly be a previously observed object, and if not, what the discrepancy is. There are many distance- or pseudo-distance metrics that may be used to measure the distance between two state distributions (e.g. Mahalonobis distance). Problematically, none of these distance metrics directly quantify the level of propulsive effort required to effect the observed state change. This difference is critical, as very small fuel expenditures at specific points in an orbit can produce outsized state discrepancies.

This study uses a minimum-fuel control distance metric and hypothesis testing to approach data association, maneuver detection and characterization problems. Because on-board fuel remains a scarce commodity for operational spacecraft, operators are likely to execute optimal or near-optimal maneuvers. Under the assumptions of optimal control, multiple deterministic observations can be related by computing the control effort required for a spacecraft to meet those boundary conditions. This approach necessitates the reconstruction of a minimum-fuel trajectory consistent with a-priori information and new observations, supporting SSA maneuver characterization needs. Optimal connecting trajectories are computed in a MATLAB minimum quadratic control trajectory optimization implementation of trajectory optimization software. The resulting optimal trajectory is used as an input in the proposed hypothesis testing framework, incorporating anomaly detection results from the previous papers [6, 7, 8]. The combined framework is tested using simulated and real-world operational data to validate the method and evaluate any limitations. Finally, the results from these simulation cases are compared to data association approaches using other distance metrics.

2.1 Statement of Work

The original Statement of Work (SoW) for this effort is enumerated below. Each SoW element is explicitly identified in the appropriate sections of this report. Minor modifications to the SoW agreed upon by the Program Manager and Principal Investigator (PI) are identified and described in footnotes where appropriate.

1. **Framework Implementation.** Incorporate existing theory accounting for boundary condition uncertainty and anomaly detection hypothesis testing. In particular, the prototype code used to generate results in previous literature will be rewritten to accommodate more general test cases and data inputs.[1]

2. **Compare Results.** Compare the control distance metric data association techniques against other data association approaches (e.g., Mahalanobis distance, orbit element gating) using simulated data[2]. After the proposed approach has been implemented and internally tested, the results will be compared with previously proposed and currently used approaches such as Mahalonobis distance and orbit element gating. As the project progresses, different data association methods will be compared.

3. **Extend Theory**[3]. The theoretical approach to reducing variational cost conservatism will be pursued using analytical methods. After a satisfactory theory accounting for boundary condition variations has been developed, it will be compared with both the more

[1] For programmatic purposes, the development, implementation, and inclusion of trajectory optimization code was also added to the effort.
[2] During the performance period of this effort the empirical WAAS data became available and a similar analysis with this data is included in this report.
[3] The Galaxy 15 trajectory information in the WAAS data presumes an electric thruster propulsion system; trajectory fuel cost function modifications were unnecessary for this effort. An extension of the theory to allow for Gaussian Sum representations of the boundary constraint uncertainties is included instead in Appendix B.

conservative quadratic cost upper bound and the unscented transform approach recently developed in the literature.

The remainder of this report addresses these SOW items as follows: SoW item 1, 'Framework Implementation,' is discussed in section 2.2, DAMMM Overview, SoW item 2, 'Compare Results,' is addressed in section 3.0 and 4.0, and SoW item 3, 'Extend Theory,' is discussed in Appendix B.

2.2 DAMMM Overview

To address this research goal, the algorithm framework (and MATLAB software block diagram) is defined in Figure 1 and described below. The variables of Figure 1 are as follows: $x_{\mu,A}$ is the mean state of the observation at t_A, $x_{\mu,B}$ is the mean state of the observation at t_B, $P_{x,A}$ is the covariance of the observation at t_A, $P_{x,B}$ is the covariance of the observation t_B, $\mathbf{x}^*(t)$ is the optimal state trajectory, $\mathbf{u}^*(t)$ is the optimal control trajectory, $\mathbf{p}^*(t)$ is the optimal costate trajectory, J_{nom} is the quadratic control cost of the optimal trajectory, f(J) is the quadratic control cost distribution, and P_H is the probability of anomaly. This software framework and associated code documentation in Appendix A constitute the work satisfying the 'Framework Implementation' SoW item in section 2.1. The inputs to the algorithm are two UCTs, containing the estimated states of the trajectory boundary conditions along with covariance matrices describing the probability distribution of these boundary states. The first portion of the algorithm simply parses the input tracks to extract the nominal boundary states at the initial point (labeled as point A in Figure 1) and final point (B) and stores the covariance data for use later.

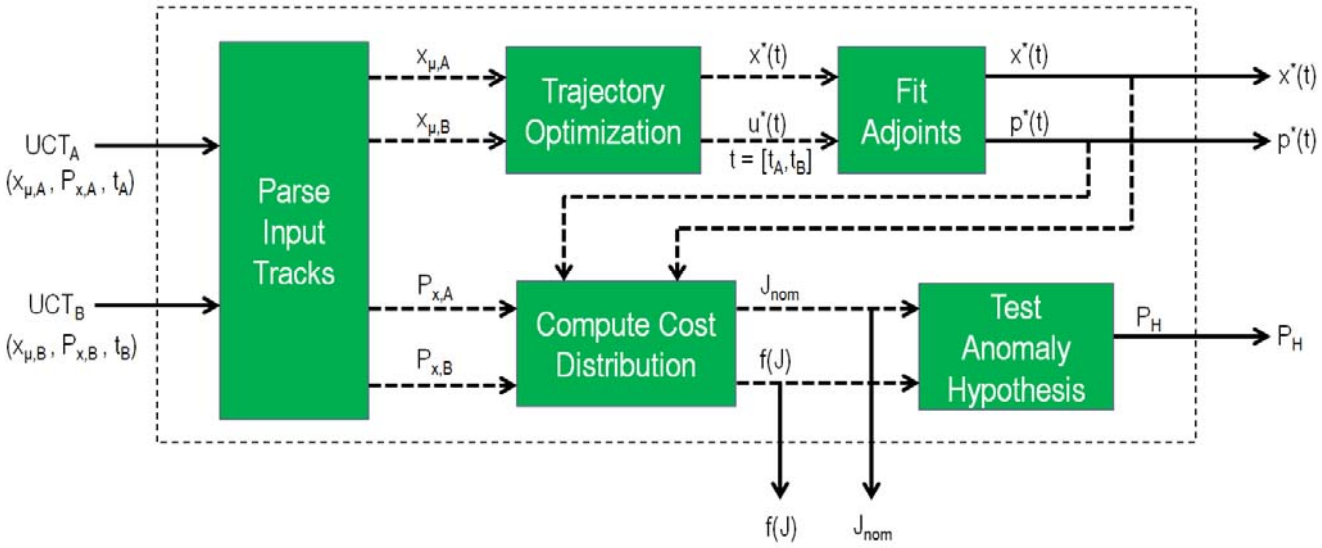

Figure 1. DAMMM Algorithm Functional Flow Diagram

The nominal states are used to generate an optimal trajectory that connects the boundary points through the trajectory optimization algorithm. This algorithm solves the deterministic two-point boundary value problem using MATLAB's constrained minimization function, *fmincon*. The cost function being minimized, shown in Equation 1, is the quadratic control cost (J), which

is a function of the control thrust accelerations (u) and is ideal for variable specific impulse engines (VSI):

$$J = \tfrac{1}{2} \int \mathbf{u}^T \mathbf{u} \, dt \tag{1}$$

The initial and final points are used as boundary conditions and the simulation time is discretized into a user-defined number of intermediate steps. The decision variable for this minimization is a stacked vector of the thrust acceleration vectors at each discrete time instant. Keplerian two-body dynamics are enforced between steps of the trajectory as equality constraints to ensure the generated trajectory dynamics are accurate. Because the partial derivatives of the dynamics with respect to the decision variables (thrust accelerations) are well known, the gradient of the constraint is supplied to the optimization algorithm, greatly improving performance of the implementation. The output of this step is a nominal optimal state and control trajectory connecting the UCTs. The generated optimal trajectory is validated using the nonlinear dynamics to numerically integrate the proposed control vector and quantify the error between the integrated final condition and the specified final UCT boundary condition. Adjusting tunable convergence parameters of the optimization algorithm, such as absolute and relative tolerances, can reduce this error. For this study, the relative and absolute convergence criteria are both set to 10^{-12} to decrease final state error. The well-behaved nature of the dynamics allows solutions to even this low tolerance on the order of tens of steps, so the effect on computational tractability is minimal. For instance, over 100 test runs of the nominal simulated trajectory (defined in Section 3.1), the trajectory optimization routine ran 5 iterations of the optimizer before converging, with an average runtime of 0.314 seconds. The computer used for this test is an i5-2500K clocked at 4.2 GHz with 16 GB random access memory (RAM) running 64-bit MATLAB 2013a.

The optimal states $\mathbf{x}^*(t)$ and controls $\mathbf{u}^*(t)$ for $t_A \leq t \leq t_B$ are then used to estimate a history of optimal control costates $\mathbf{p}^*(t)$. This step is required because algorithm that computes the control cost distribution requires costates instead of thrust accelerations. The costates are constructed iteratively by guessing a costate trajectory based on the optimal control trajectory and then modifying the costates through iterative least-squares method until the control cost is within a user-defined convergence tolerance of the optimal trajectory. As an additional check, the new optimal costate trajectory is compared to the original optimal trajectory to ensure the endpoint error has not changed significantly.

Using the optimal state and costate trajectories, as well as the covariance information from the input tracks, control probability distributions are generated using the techniques outlined in a previous paper [8]. Finally, the nominal optimal control cost and control distribution are used to test the hypothesis that a maneuver actually occurred and complete the maneuver detection task.

3.0 METHODS, ASSUMPTIONS, AND PROCEDURES

As described in section Section 2.2, each UCT pair combination examined in this study is considered a Two-point Boundary Value Problem (TPBVP). The trajectory optimization is performed to generate a nominal optimal trajectory connecting the two boundary conditions (UCTs). Presently, Keplerian two-body dynamics are assumed and other perturbations are ignored (e.g., lunar, solar, non-spherical perturbations). For each case tested, a nominal UCT boundary condition uncertainty (covariance matrix) is parameterized using a scalar multiplier to examine the effects of uncertainty on anomaly detection. Similarly, to examine the effects of

time separation between UTCs, each scenario simulates various time intervals between UCTs of up to 48 hours. The resulting control cost distributions due to state uncertainty at the boundary conditions are approximated using the analytic first and second moments as normal distributions as specified in Holzinger et al [8]. The deterministic control cost is then compared to the control cost distributions to rigorously test the maneuver / anomaly hypothesis.

Using these boundary conditions, a deterministic maneuver connecting UCT A and UCT B is computed. After generating the nominal optimal control trajectory and the corresponding costate trajectory ($\mathbf{x}^*(t)$ and $\mathbf{p}^*(t)$), uncertainties in position and velocity are used to generate an approximate probability distribution of the control cost. The position and velocity uncertainty values used in this simulation are shown in Table 1. The mean of the total cost distribution (μ_p) is equal to the optimal nominal control cost (J^*) plus the minimum detectable cost for a given uncertainty condition, where the minimum detectable cost is calculated from the state uncertainty boundary conditions. The process for calculating the mean (μ_p) and standard deviation (σ_p) from the optimal trajectory and covariance is based on Equations 2 and 3 respectively. The details of the derivation of these equations are in the previous paper [8] with Tr being the trace operator.

$$\mu_p = J^* + \mathrm{Tr}[\mathbf{\Omega P_z}] \tag{2}$$

$$\sigma_p = \boldsymbol{\omega}^T \boldsymbol{P}_z \boldsymbol{\omega} + 2\mathrm{Tr}[\mathbf{\Omega P_z \Omega P_z}] \tag{3}$$

Here, $\mathbf{P_z}$ is a 12-by-12 matrix with the initial and final covariances on the upper-left and lower-right 6x6 block diagonals, $\mathbf{\Omega}$ is the term in the performance function corresponding to the quadratic in the perturbation term (Equation 15 in Reference 8), and $\boldsymbol{\omega}$ is the term in the performance function corresponding to the cross-term between the nominal control distance and perturbation (Equation 14 in Reference 8). Furthermore, the minimum detectable quadratic cost is used to determine if state uncertainty accounts for the state change, and is defined as the mean of the cost distribution generated from state uncertainty, shown in Equation 4 (using terms from Equation 2):

$$J_{det} = \mathrm{Tr}[\mathbf{\Omega P_z}] \tag{4}$$

In order to better model the cost distribution, an exact distribution is also constructed using a Monte-Carlo approach using a random vector $\delta \boldsymbol{Z} \in N(\mathbf{0}, \boldsymbol{P}_z)$. The quadratic cost due to this state uncertainty can then be calculated as shown in Equation 5 [8]:

$$J_{unc} = \boldsymbol{\omega}^T \delta \boldsymbol{Z} + \delta \boldsymbol{Z}^T \mathbf{\Omega} \delta \boldsymbol{Z} \tag{5}$$

Ten-thousand costs were sampled and binned into 1000 bins to construct a distribution of costs. The minimum detectable cost for this distribution is then found by computing the normalized Probability Density Function (PDF) and Cumulative Distribution Function (CDF). The cost where the CDF for this control distribution equals 0.5 is defined as the minimum detectable control cost. While both Gaussian approximate and Monte-Carlo distributions are generated, the resulting distributions are nearly identical, so the remainder of the report uses the (more accurate) Monte-Carlo distribution.

A trajectory with a nominal control cost J^* greater than the minimum detectable cost J_{det} has a higher probability (greater than 0.5, asymptotically approaching 1 as J^* increases) of being

the result of a controlled maneuver or unmodeled perturbation and not just the result of propagated boundary condition uncertainty.

The probability that a hypothesis is true (p_A) can be computed from the distribution of costs ($f_{J^*}(J^*)$) as shown in Equation 6 [7]:

$$p_A = \int_{-\infty}^{J^*} f_{J^*}(J^*)\mathrm{d}J^* \tag{6}$$

A sample result from this method (using the synthetic scenario defined in Section 3.1) is shown in Figure 3. The figure shows the PDF and CDF for the quadratic control cost as a function of control cost. The maximum value of the normalized PDF corresponds to the minimum detectable cost as defined in Equation 4, and the vertical dashed line represents the nominal optimal control cost for that maneuver. On the CDF plot, it can be seen that the intersection of the CDF plot and nominal quadratic cost yields a probability of anomaly of approximately 0.75, or 75%. Indeed, the CDF is the key to computing the probability that a maneuver has occurred for a given optimal trajectory and state uncertainty. This probability of a maneuver occurring is also referred to as the probability of anomaly, denoting the possibility that anomalous behavior outside the assumed dynamics (e.g. a maneuver or unmodeled perturbations) are the cause for the state change.

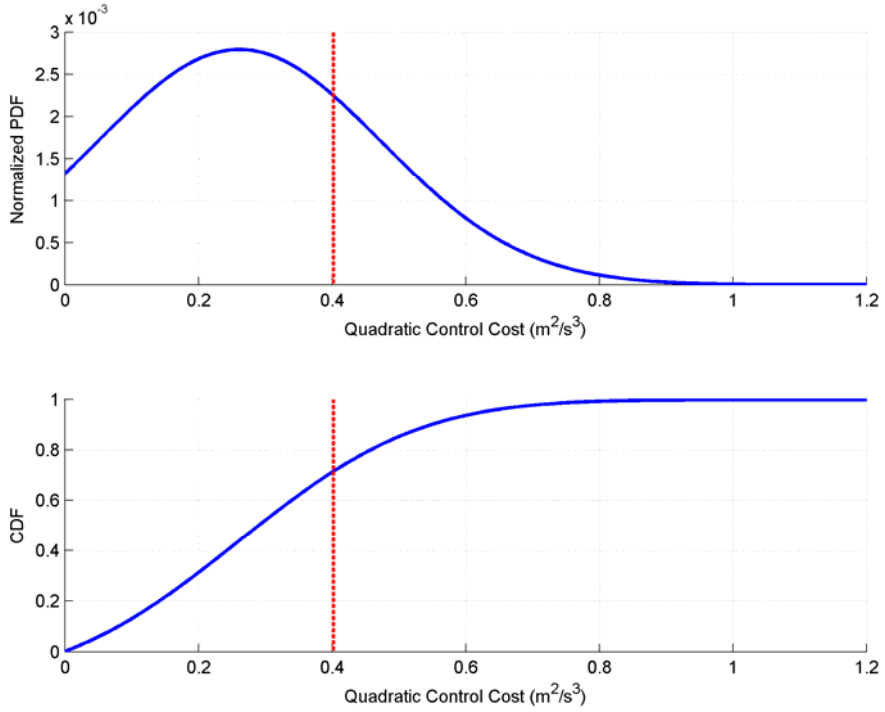

Figure 2. Normalized PDF and CDF vs Difference From Minimum Detectable Control Cost

Since the control cost and distribution varies for each time horizon and UCT uncertainties, it is more intuitive to define and use a Signal-to-Noise Ratio (SNR) as the ratio of the nominal optimal control cost to the minimum detectable cost, as shown in Equation 7:

$$SNR = \frac{J^*}{J_{det}} = \frac{J^*}{\mathrm{Tr}[\boldsymbol{\Omega P_z}]} \tag{7}$$

If the nominal optimal control cost (the signal) is equal to the minimum detectable quadratic cost for a given state uncertainty (the noise), then the SNR is unity. When SNR = 1, the probability of anomaly is equal to 0.5, or 50%. That is to say, there is an equal probability that the observed state change is caused by an anomaly (such as a control maneuver) or caused by uncertainty in the initial and final states. As the nominal cost increases with respect to the minimum detectable cost, the SNR increases and the probability that the state change is caused by an anomaly increases. As SNR increases, the nominal cost becomes substantially larger than the cost uncertainty, so the probability that state uncertainty could cause the state change is zero and the probability of anomaly approaches 1.0, or 100%.

Given an optimal trajectory and uncertainty in the boundary conditions, one can compute the likelihood that the observed state change (or lack thereof) is due to quiescent propagation or active maneuvering, thus addressing the maneuver detection goal. This final step in the DAMMM procedure is referred to as testing the anomaly hypothesis, as shown in Figure 1. Additionally, if it is determined that boundary condition uncertainty cannot account for the state change, and a maneuver or unmodeled perturbation must have occurred, the minimum magnitude and time history of the potential maneuver can be computed, characterizing any such maneuver. Furthermore, if the maneuver is determined to be impossible given the assumed propulsive capability of the RSO, this method can be used to associate (or disassociate, in this case) UCTs based on the control authority required.

The first part of SoW item 2, 'Compare Results,' is to validate the software implementation. To do so, extreme test cases are used to identify the limits and performance of this approach in non-ideal situations. Primarily, the process sensitivity to boundary condition uncertainty and simulation duration must be understood to better utilize and interpret the results of the algorithm. Increasing state uncertainty decreases the SNR (minimum detectable cost increases), and it is important to know what SNRs yield reliable results. Additionally, simulation duration (the time between initial and final boundary conditions) affects the performance of the trajectory optimizer, and the problem of correlating UCTs over large time periods is particularly difficult when objects maneuver during gaps in observations.

To validate the software implementation, a sensitivity study is conducted to generate confidence curves of probability of anomaly based on a) maneuver SNR and b) UCT time separation. The boundary condition uncertainty is initialized at 1 meter in position and 0.01 meters-per-second in velocity, as shown in Equation 8:

$$\boldsymbol{P_A} = \boldsymbol{P_B} = \text{diag}(\alpha^2, \alpha^2, \alpha^2, (0.01\alpha)^2, (0.01\alpha)^2, (0.01\alpha)^2) \,, \tag{8}$$

where α is the scalar that is varied between scenarios to change the uncertainty (and modulate the effective SNR). The scalar was allowed to vary logarithmically from 1 to 10^5, determined by trial and error to cover a wide range of SNR values (from near-zero to above 6). This corresponds to position and velocity uncertainties of 100 km / 1 km/s at maximum, and 10m / 0.1m/s at minimum. The simulation duration between UCTs is varied as well, keeping the ascending node passage at the midpoint of the simulation duration. The initial and final times are varied from 5 minutes before and after the ascending node respectively (10 minute simulation duration) to 24 hours before and after the ascending node respectively (48 hour simulation duration). The results of this study, as well as the nominal 1-hour duration case, are included in Section 4.1.

3.1 Scenario Descriptions

To validate the DAMMM framework, two scenarios are considered. First, a synthetic data (simulated) scenario is constructed with a geostationary spacecraft executing a one-degree inclination-change maneuver at the ascending node. This particular scenario was chosen to replicate the available WAAS data for the Galaxy 15 geostationary spacecraft. The second scenario uses the WAAS data, which enables examination of Galaxy 15 N-S (inclination) electric thruster station-keeping maneuvers. This process illustrates a possible operational use-case of the software package and identifies how the proposed DAMMM framework for maneuver detection, characterization, and UCT correlation can work. Each scenario is described individually in the following subsections.

3.1.1 Synthetic Data Scenario.

The synthetic (simulated) scenario is constructed to emulate an inclination-change station-keeping maneuver, such as the operational case provided in the WAAS data. The boundary conditions for this simulation can be seen in Table 1. A spacecraft is initialized in a circular orbit at GEO with an initial inclination of one-degree. The final state has an identical semi-major axis, eccentricity, and right ascension of the ascending node, now has zero inclination. Note that, since this orbit is circular, the argument of periapsis is undefined. Notice also that the true anomaly changes by roughly 15 degrees during the simulation. At GEO, this approximately corresponds to a one-hour simulation duration. The initial condition (UCT A) occurs 30-minutes before the spacecraft crosses the ascending node (where the maneuver is executed), and the final condition (UCT B) occurs 30-minutes after the ascending node crossing. A time-step of one minute between each discrete step of the simulation is selected, so the simulation is divided into 61 equal steps. Figure 3 shows the inclination approaching the target value over the course of the simulation, as well as the commanded control (thrust acceleration), in meters-per-second.

Table 1. Simulated Scenario Boundary Conditions

Parameter	Initial Condition (UCT A)	Final Condition (UCT B)	Units
Semi-major Axis	42164	42164	kilometers
Inclination	1	0	degrees
Eccentricity	0	0	-
Right Ascension of Ascending Node	0	0	degrees
Argument of Periapsis	n/a	n/a	degrees
True Longitude	352.4795	7.5205	degrees
Position Uncertainty	1α	1α	meters
Velocity Uncertainty	0.01α	0.01α	meters-per-second

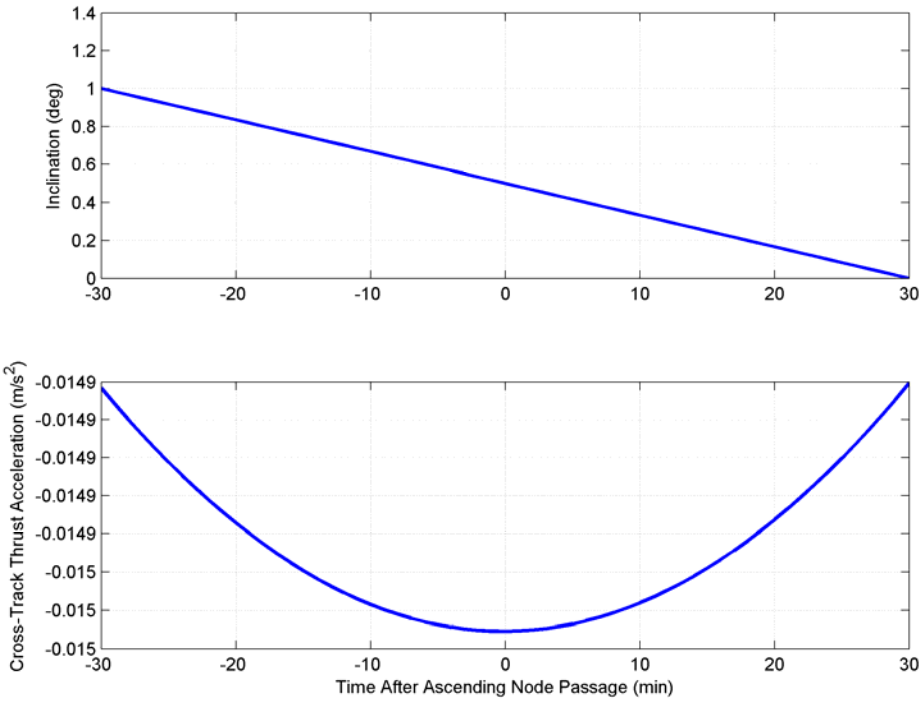

Figure 3. Sample Trajectory and Control for Plane Change Maneuver

The synthetic data scenario is used in two analyses in this study. The first is the specific test case detailed above, with varying state uncertainty, testing the outcome of the anomaly hypothesis process. The second is a sensitivity study, meant to extend the algorithm to longer duration simulations and more extreme SNR situations, to test the algorithm capabilities.

3.1.2 Real-World Data

To complement the simulated scenario, the algorithm is tested using real operational data supplied by Captain. Kulumani and Dr. Baldwin at the Air Force Research Laboratory (AFRL) Space Vehicles Directorate. The availability of this real-world data drove the construction of the simulated scenario in Section 3.1.1. The data, taken from observations of the Galaxy 15 geostationary satellite, spans the month of February 2014, and includes Earth-centered Earth-fixed (ECEF) position and velocity, as well as radial, in-track, and cross-track (RIC) acceleration (as seen by a rotating Hill frame attached to the spacecraft). Inspection of the acceleration data, shown in Figure 4, reveals two candidates for the North-South (inclination) station-keeping maneuver: one during February 9th, and another during February 23rd. Both candidates show a large anomalous cross-track acceleration (seen in the bottom plot of Figure 4), which is indicative of a plane change maneuver and therefore a station-keeping maneuver.

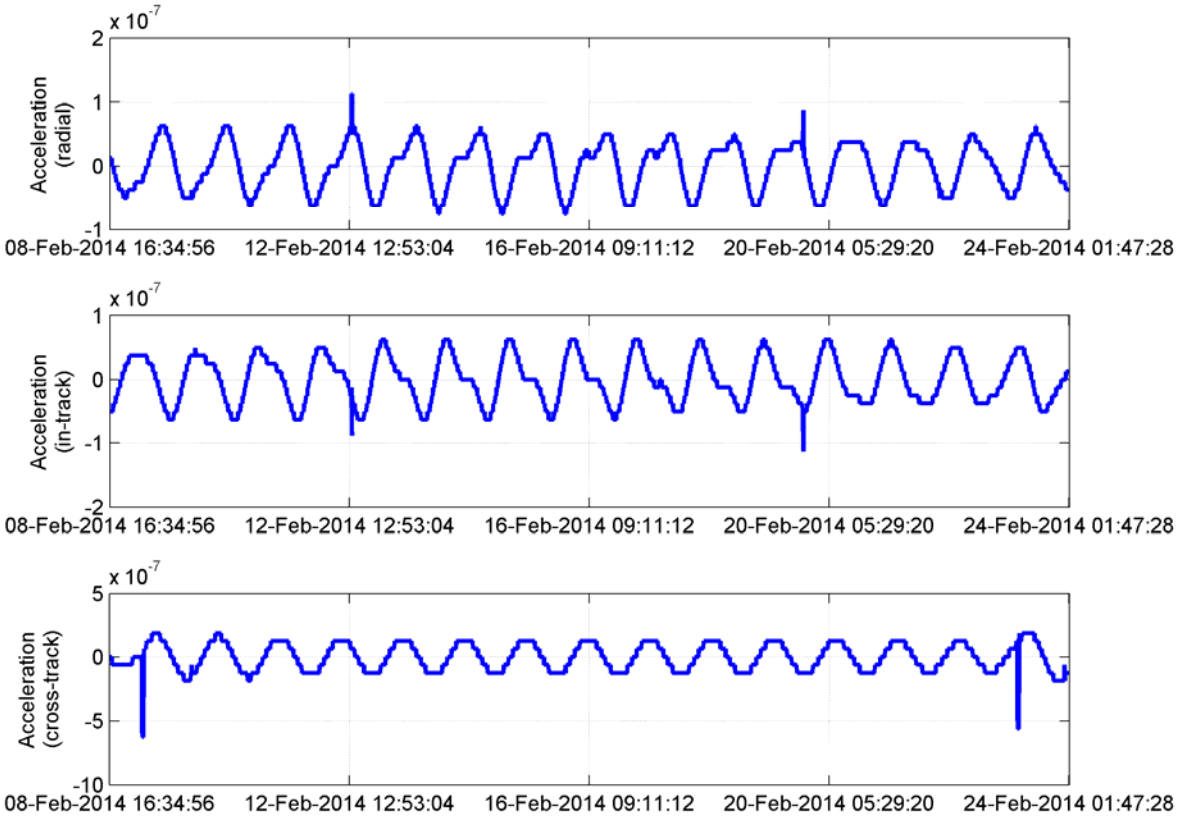

Figure 4. RIC Acceleration Data of Galaxy 15 from WAAS Data

The data is analyzed in a similar manner to the synthetic data sensitivity study: by varying boundary condition uncertainty and time, a sensitivity study is conducted to construct probability of anomaly confidence curves with respect to SNR and simulation duration. From the two candidate maneuvers, the initial boundary condition is selected as the February 8th maneuver, just before the large cross-track thrust. This initial boundary condition is held fixed, and the final state and simulation duration are changed by choosing different final boundary condition states. Therefore, the study begins with a simulation duration of 1 hour and increasing to a duration of 48 hours. The results of this sensitivity study are included in Section 4.2.

4.0 RESULTS AND DISCUSSION

The results from this effort are broken down into numerous sections, addressing various portions of the proposed work. The results from the simulated scenario are discussed to validate the minimum-fuel distance metric approach to maneuver detection. Similarly, the real-world data is used to test the application of the software suite to a plausible operational situation (part 1 of SoW item 'Compare Results'). The minimum-fuel distance metric approach is also compared to other common distance metrics to assess its usefulness, particularly in spacecraft in maneuver detection (part 2 of SoW item 'Compare Results').

4.1 Framework Validation

The simulated one-hour, one-degree GEO inclination correction maneuver, as defined in Table 1 and Section 3.1, is used to validate the DAMMM algorithm, ensuring functionality of the algorithm as shown in Figure 1. The resulting nominal simulated maneuver trajectory is shown in orbit-element space in Figure 2, showing the 1-degree inclination correction. The quadratic cost for this maneuver is shown in Table 2. Using the control history obtained from the trajectory optimizer, the actual velocity change (denoted as ΔV) can be computed as the integral of the thrust accelerations over time. As a sanity check, this velocity change is compared to other bounding costs for validation. For instance, any non-impulsive maneuver is bounded from below by the impulsive equivalent of that maneuver. The velocity change required for an impulsive 1-degree inclination change at GEO is shown in Table 2, and optimal trajectory is bounded from below by the impulsive cost as expected. Additionally, an upper-bound cost can be applied based on the quadratic cost from the maneuver [9]. The value of the upper bound for this scenario is also shown in Table 2. The trajectory cost is within the acceptable range for both of these checks.

Table 2. Simulated Maneuver Control Cost and Comparisons

Parameter	Value	Units
Quadratic Control Cost	0.4022	m^2/s^3
Impulsive ΔV	53.6624	m/s
Actual ΔV	53.8151	m/s
Upper-bound ΔV	53.8153	m/s

Using the nominal optimal trajectory for this scenario, uncertainty is introduced in the initial and final UCTs. The initial and final UCTs are each initialized with 1-meter position uncertainty and 0.01-meter-per-second velocity uncertainty. Notice that the velocity uncertainty is much smaller than the required velocity change from Table 2, so intuition says that this condition is highly observable and the probability of anomaly is 1. Indeed, this is the case as the nominal SNR for this case is very high. The uncertainties were then scaled together up to 10^4 times the initial amount in order to increase the position and velocity noise, for a maximum position and velocity uncertainty of 100 kilometers and 1 kilometer-per-second, respectively. Figure 5 shows the result of the variation of the probability of anomaly as a function of SNR. As desired, the probability of anomaly at an SNR of 1 is exactly 0.5, so there is an equal likelihood that the observed state change is caused by a control maneuver or uncertainty. As SNR increases above 1, the likelihood that a maneuver occurred increases, and vice versa below an SNR of 1. It can be noted that above an SNR of 6 the probability of anomaly is always 1, so the plots have been truncated to only show the interesting lower ranges of SNR. Given the results from this simulated scenario, if the SNR is above 2, the algorithm would say that there is a high likelihood that either the object seen has maneuvered or the tracks are not correlated and actually belong to separate objects. In order to make this association distinction, prior information on the object and the propulsive requirements from the optimal trajectory should be considered. This nominal simulated scenario has shown that the DAMMM algorithm is capable of ingesting UCT data (states and distributions) and utilizing knowledge of orbital mechanics to provide data to aid in the association of the tracks.

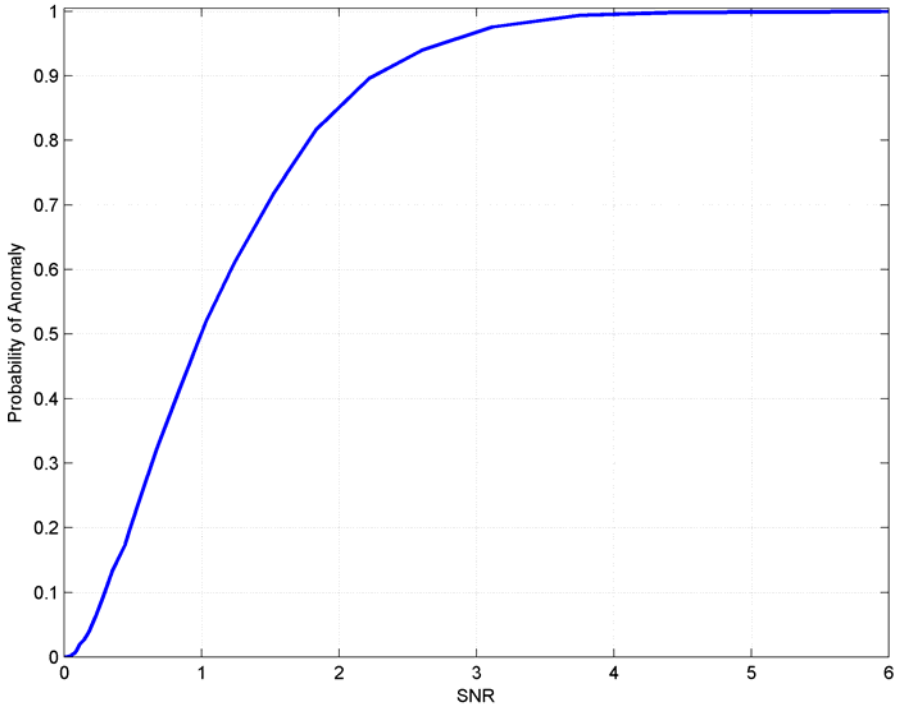

Figure 5. Probability of Anomaly vs. SNR, Simulated Scenario, 1-hour Duration

The algorithm has been shown to function well in this specific scenario, but in order to better characterize the performance of the algorithm, a sensitivity study is conducted. The variable parameters are the state uncertainty (as before) and the time between observations, otherwise known as the simulation duration, which was fixed in the previous analysis. Similar to the previous analysis, the state uncertainty was initialized at 1-meter position uncertainty, 0.01-meter-per-second velocity uncertainty, and was scaled up to 10^5 times to vary SNR. The uncertainty had to be varied so drastically because the minimum detectable quadratic cost varies widely with changes in simulation duration. Simulation durations varied between 10 minutes and 48 hours, varying evenly on either side of the ascending node crossing.

4.2 Synthetic Data Parametric Performance

Figure 6 is a contour plot containing the results from this investigation; SNR and duration are varied on the x- and y-axes respectively, and the contours show lines of constant probability of anomaly. The contours shown represent different increasing probabilities of anomaly that the maneuver would be observed given the observation duration and uncertainties. Once again, the 0.5, or 50%, confidence level is a straight line at an SNR of 1, as expected due to the nature of the anomaly detection method. The results show a relatively low impact of simulation duration on the detectability of the maneuver since the confidence contours are mostly straight lines. The major exception to this occurs at simulation durations of 12 and 36 hours, which correspond to the initial and final conditions with the highest out-of-equatorial-plane state difference between the observations. At these points in the orbit, smaller boundary condition uncertainty is required to be able to conclude that a maneuver has indeed occurred. However, for even 75% confidence in maneuver detection, the SNR required is never greater than 2.

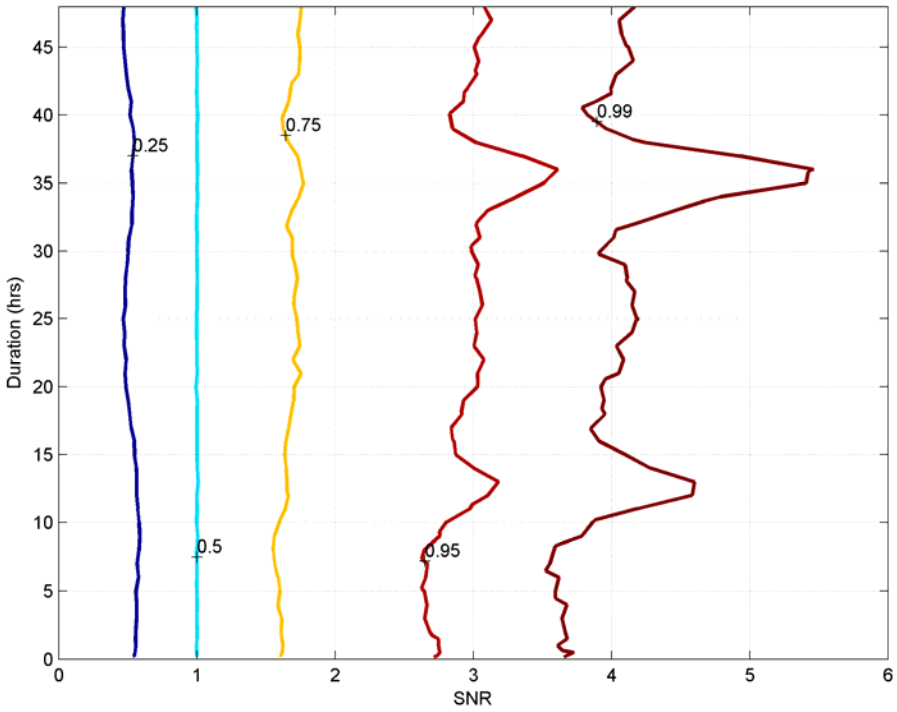

Figure 6. Anomaly Detection Probability Confidence-level Contours for Uncertainty and Duration Sensitivity Study, Synthetic Scenario

This result emphasizes an advantage of the control metric approach, which is that it performs consistently with respect to observation duration. Some previous knowledge of the orbit is still useful in determining the validity of the maneuver detection probability results. For instance, when attempting to detect inclination change maneuvers, observations spaced at half-orbit periods are not ideal because this is could yield a large state difference and require lower observation uncertainty to detect maneuvers with high likelihood. Another, more obvious, result is that larger maneuvers, which yield a higher SNR for the same boundary condition uncertainty, are easier to detect. This is particularly relevant for maneuvers by spacecraft with variable specific-impulse engines, where the state changes are small and spread out over a long time. Conversely, a large state-change by a nearly-impulsive maneuver could still be detected even in a short time between observations, if the control required for the maneuver significantly exceeds the state change in the homogenous orbit based on boundary condition uncertainty.

4.3 WAAS Data Parametric Performance

To further investigate the effectiveness of this algorithm, and to apply it to a situation representative of operational situations, real data was obtained from AFRL and used in the algorithm as described in Section 3.2. The data obtained was from roughly one month of observations (during February 2014) of the Galaxy 15 spacecraft in geostationary orbit. This spacecraft features an IHI BT-4 propulsion system, which performs as a variable specific-impulse engine, so the results should be in line with section 4.1. The data was examined to pick out point in time where a station-keeping maneuver likely occurred, determined by the

acceleration data shown in Figure 4. As discussed in Section 3.2, the initial boundary condition was chosen as a state just before the large cross-track acceleration observation on February 8th. Beginning with this point, the final condition was selected by increasing the duration between observations, up to 48-hour simulation duration. The state uncertainty was varied similar to the simulated case, beginning with 1-meter position uncertainty and 0.01-meter-per-second velocity uncertainty and scaling up to a factor of 10^5 times to vary SNR.

The results of this sensitivity study are shown in Figure 7. The confidence-level contours show similarities with Figure 6 from the synthetic scenario. The 0.5 confidence level is once again a straight line at a SNR of 1, as prescribed by the method. In this case, though, the probability of detection is even more consistent. This is likely because of the differences between the modeled dynamics and real system. The simulation assumes Keplerian two-body dynamics, whereas in reality many accelerations are acting on the RSO, including n-body gravitational effects, non-spherical gravitational perturbations, and solar radiation pressure. As seen in the acceleration data in Figure 4, the spacecraft is thrusting continuously, likely rejecting some of the perturbations to maintain its orbit slot. Due to this constant maneuvering and unmodeled dynamics, there is less correlation between states with half-orbit-period observation time differences than in the simulation. Therefore the nominal control cost required to associate UCTs is more consistent throughout the orbit.

The WAAS data was also sampled with a lower duration between observations, with an average 20-minute duration increase between the sampled WAAS data points. The agreement between the simulated and operational data cases reinforces the applicability of this algorithm to real data. Even given the simplifications in the algorithm, notably the Keplerian two-body dynamics assumptions of the trajectory optimization step, the results from using real data set closely resemble the simulated example. This lends confidence to the application of this algorithm to operational data.

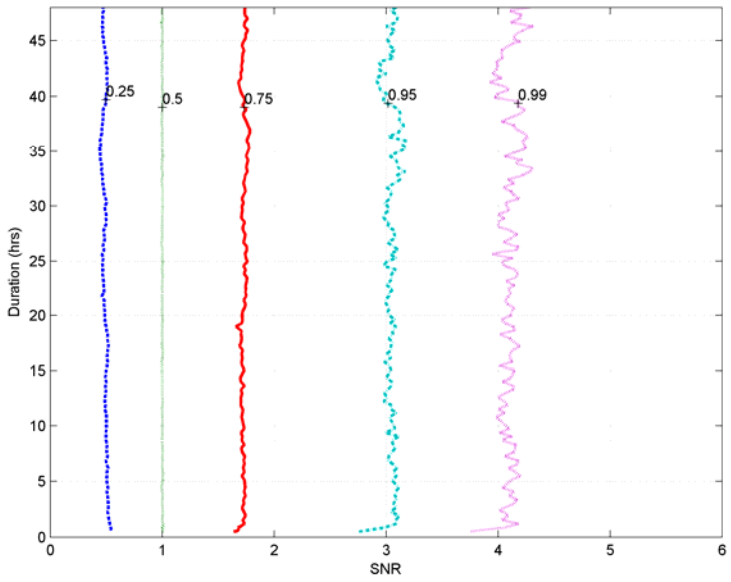

Figure 7. Anomaly Detection Probability Confidence-level Contours for Uncertainty and Duration Sensitivity Study, WAAS Data

4.4 Comparisons to Other Distance Metrics

The proof of control performance as a metric is shown in the previous work by proving the properties of positivity, strict positivity, symmetry, and triangle inequality [8]. In order to assess the effectiveness of the control cost as a distance metric, it is important to consider comparisons to other common distance metrics. Primarily, it is important to note the differences between control cost and both geometric and multivariate distribution distance metrics, and the advantage that a control cost metric lends in orbital mechanics applications.

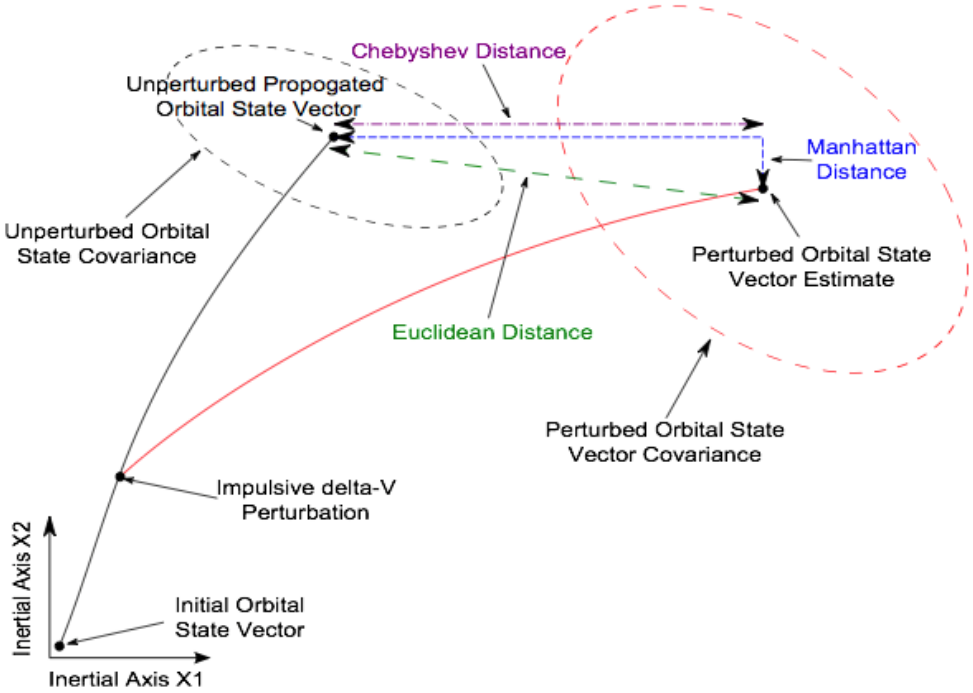

Figure 8. Geometric Distance Metrics Applied to Maneuvered Object Correlation

A pictorial example of geometric distance metrics is included in Figure 8. The most common geometric distance metric for evaluating the difference between two orbital state vectors is Euclidean distance. This considers only the position difference between two different states without consideration for uncertainty in the boundary conditions. The Euclidean distance is calculated by taking the 2-norm of the difference in position, expressed in Equation 9:

$$d_E(\boldsymbol{x}_A, \boldsymbol{x}_B, t_B) = ||[\boldsymbol{I} \quad \boldsymbol{O}](\boldsymbol{x}_B - \boldsymbol{x}_A(t_B))||_2 \ , \tag{9}$$

where $\boldsymbol{x}_B$ is state vector of the final UCT and $\boldsymbol{x}_A(t_B)$ is the state the initial UCT state propagated to time t_B. The quiescent propagated state $\boldsymbol{x}_A(t_B)$ is calculated by taking the initial condition UCT and propagating it under the assumption that no maneuver has been performed. In Euclidean distance, only the positional difference is considered in relating the two states. For observation association in the space environment, this is not a good method since even a small control input can cause a large positional diversion over time. For instance, a spacecraft that performs a plane change maneuver at the ascending node will have a small positional difference between the

perturbed and homogenous orbits at first, but after a quarter of an orbit period the out of plane displacement will be significant. Furthermore, depending on the time of observation, objects in very different orbits reside close in position. In each of these cases, a geometric distance metric would have a difficult time of correctly associating uncorrelated tracks.

Alternately, metrics that measure the distance between multivariate normal distributions, such as an orbital state vector, can take into account both position and velocity information as well as uncertainty in the state vectors. This is ideal in defining a metric to discriminate between two orbital state observations. One example of such a metric is the Mahalonobis distance, which effectively applies a weight to the state difference along each axis based on the combined uncertainty along that axis in the observations [10]. The expression for the Mahalonobis distance is given in Equation 10:

$$d_M(\boldsymbol{x_A}, \boldsymbol{P_A}, \boldsymbol{x_B}, \boldsymbol{P_B}, t_B) = \sqrt{(\boldsymbol{x_A}(t_B) - \boldsymbol{x_B})^T (\boldsymbol{P_A}(\boldsymbol{t_B}) + \boldsymbol{P_B})^{-1} (\boldsymbol{x_A}(t_B) - \boldsymbol{x_B})} \ , \qquad (10)$$

where $\boldsymbol{x_B}$ and $\boldsymbol{P_B}$ are the full state and covariance information of the state estimate from the final UCT, and $\boldsymbol{x}_A(t_B)$ and $\boldsymbol{P_A}(t_B)$ are the state and covariance of the quiescent propagated state. Similar to Euclidean distance, the propagated homogenous state is calculated by taking the initial condition UCT and propagating it under the assumption that no maneuver has been performed, and the propagated covariance is calculated using the propagated state transition matrix to update the initial covariance. Mahalonobis distance improves upon Euclidean distance by accounting for uncertainty: larger uncertainty in any axis will yield a lower distance metric value. A value of 1 for the Mahalonobis distance is a 1-sigma distance (similarly, a value of 2 is a 2-sigma distance, etc.). Low values of the Mahalonobis distance yield a higher confidence in correlation of the full UCT, accounting for both the full state (position and velocity) and state uncertainty. However, Mahalonobis distance is still at its core a state differencing metric. Therefore, it still has the issue in orbital mechanics that, depending on the observation times, small control maneuvers can cause outsized state differences, and therefore is not ideally suited for orbital mechanics applications. Additionally, the Mahalanobis distance metric does not characterize maneuvers – it simply accounts for differences between two UCT states.

Both the Euclidean distance and Mahalonobis distance metrics are calculated alongside the synthetic and WAAS data sensitivity studies (presented in section 4.2 and 4.3, respectively). This allows a direct comparison of the various distance metrics. The resulting contour plot for Euclidean distance (in kilometers) is shown in Figure 9. First, it can be seen that, as expected, increasing SNR does not affect Euclidean distance, since it does not account for uncertainty. The Euclidean distance increases to a maximum at a duration of one-half orbit, when the homogenous state and maneuvered state are farthest in positional separation. The metric then decreases back toward zero at an orbit duration, when the orbits cross paths at the line of nodes. This behavior is cyclical with an orbit period. The difficulty of using Euclidean distance for UCT correlation or association can be seen as the value of the metric is very much dependent upon the time of observation, so developing thresholds for association is difficult. For instance, the Euclidean distance breaks down as an association metric when the position difference is small because it does not account for the velocity difference. Even RSOs in very dissimilar orbits (such a closed orbit and a fly-by trajectory) can reside in close proximity for a short time, so simply establishing a position threshold using Euclidean distance is not sufficient.

In contrast, the Mahalonobis distance metric plot, shown in Figure 10, is much more condensed for most duration values, so a smaller duration time-frame is also shown in Figure 10.

Here, the probability volume within the Mahalonobis Distance (MD) isoprobability surface is computed to give a confidence probability that the final state is consistent with the initial state, give both state uncertainties. It should be noted that SNR is not inherently meaningful for use with Mahalonobis distance since minimum detectable cost is not a factor in the equation (the **Ω** matrix from Equation 4 ends up being a scaling factor). However, for better comparison between all three metrics, Mahalonobis distance derived probability of anomaly was also plotted against SNR. At durations near an orbit period, the Mahalonobis distance decreases, showing that the UCTs are more closely correlated, with a higher likelihood that state uncertainty alone explains the observation difference. A maneuver is harder to detect at these points. Conversely, at the 12- and 36-hour durations, where the out-of-plane displacement is at its maximum, the Mahalonobis distance is considerably higher, showing that the observed state change likely requires a maneuver or other anomaly. Once again, this is due to the inherent state differencing in the metric, making the development of thresholds difficult for application to arbitrary UCT correlation.

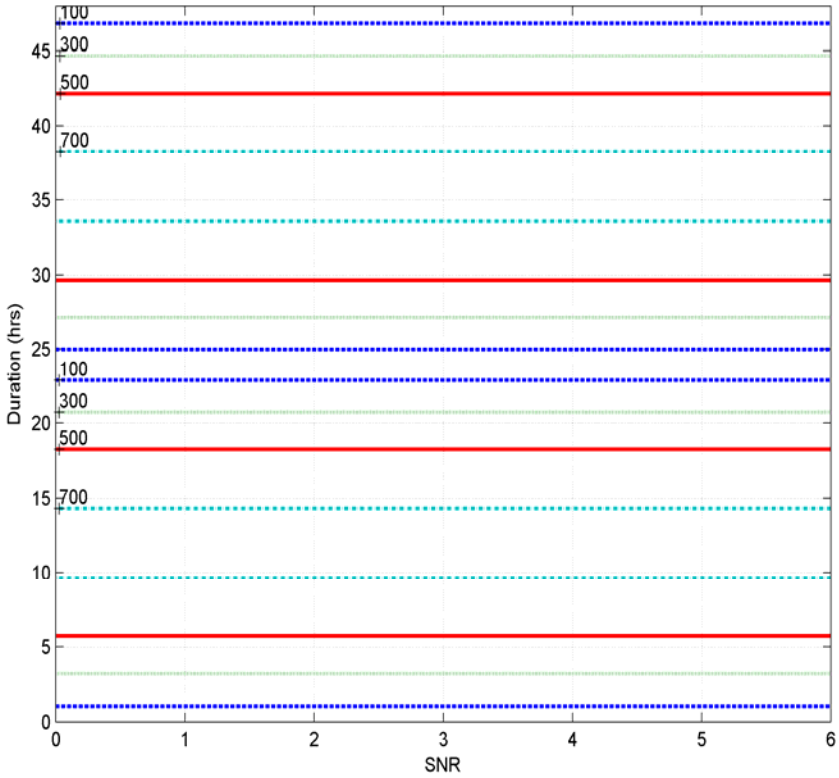

Figure 9. Euclidean Distance Metric (in km) for Synthetic Scenario Sensitivity Study

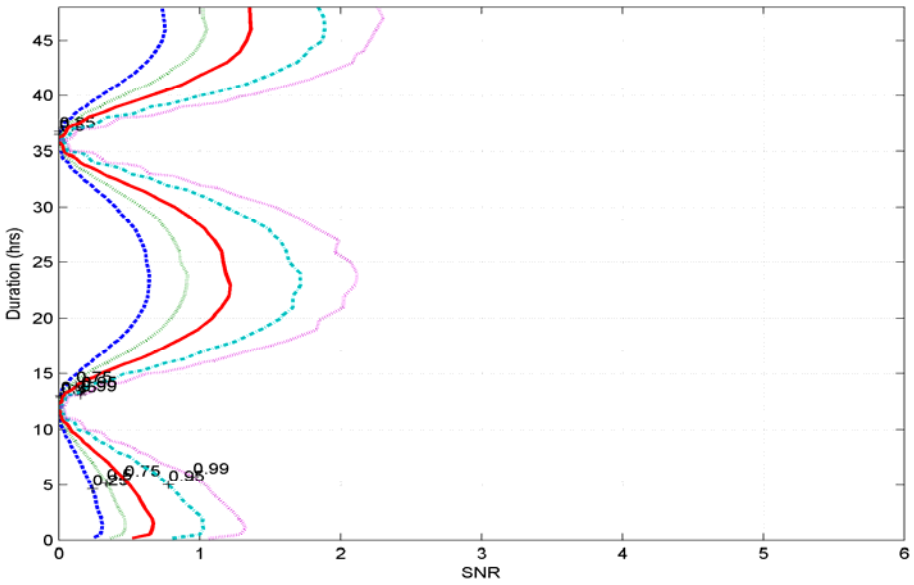

Figure 10. Mahalonobis Distance Metric for Synthetic Scenario Sensitivity Study

The advantage that the control distance metric has over these other distance metrics is that it is able to account for the specific situation of orbital mechanics when associating UCTs. As described earlier, even small control perturbations can cause a large state divergence over time, even though the orbits are actually nearly identical. All of the above metrics use state differencing to compute the distance between the observations, whereas the control distance metric implemented here considers the optimal control required to connect the tracks. In the simplest case, an un-maneuvered object should have a control distance of zero between any two points in its orbit, providing a clear indication that the tracks are correlated. In this case, the geometric or normal distribution metrics will also yield zero distance metrics because the estimated and propagated homogenous states are identical. For maneuvered tracks, however, the distance metrics described in this section do not provide a simple convention for associating tracks, as it would need to involve some level of thresholding. The control distance metric described in this study provides a natural method for correlating maneuvered tracks by computing the maneuver required to connect the tracks and accounting for uncertainty to test the hypothesis that a maneuver occurred. The only additional logic required to associate tracks is, if the probability of anomaly is high, to examine the history of the maneuver required. If the control effort required exceeds the perceived control capability of the RSO, the UCTs can be assumed not correlated, and vice versa for a reasonable control effort. Therefore, for orbital mechanics applications, the control distance metric provides an intuitive method of detecting maneuvers and correlating UCTs.

Other distance metrics, such as Mahalonobis distance, are commonly used in UCT correlation, and perform well in detecting whether two UCTs are related by their states and uncertainties. Mahalonobis distance can be useful for sensing maneuvers or unmodeled dynamics, as the distance will increase drastically; however, it cannot provide much more information. Therefore, if the task is simply to detect whether a maneuver has occurred,

Mahalonobis distance is adequate. In comparison, the control distance metric presented here provides an anomaly detection capability that is more consistent with observation duration and takes into account orbital dynamics. Additionally, since the nominal trajectory must be computed, the trajectory connecting the UCTs is also obtained in the process, which can be reviewed to inspect realism and feasibility of the anomaly hypothesis.

The differences between the metrics lend themselves to different applications. Consider a scenario where three space objects are detected in close proximity. At a later observation, three objects are also detected, but some or all of them have modified orbit element slots. Mahalonobis distance could be used to hypothesize whether the objects had indeed maneuvered, based on state differences and uncertainty, but it merely provides a statistical similarity set of the data. For instance, Mahalonobis distance cannot account for maneuvering objects. With control distance metrics, the same information and more can be gathered. The trajectories required to connect each UCT can be calculated, providing an ordered pair of the most likely correlations and their respective trajectory or maneuver requirements. In the three-RSO scenario, the UCT combinations that yield the lowest total control cost would be the most likely correlations, and the connecting trajectories can be reviewed to confirm the hypotheses.

In addition to comparisons between metrics with synthetic data, the metrics were used to investigate maneuver detection in the WAAS data. The Euclidean distance metric plot, shown in Figure 11, bears resemblance to the synthetic data plot; the oscillations are smaller in magnitude in this case, but the Euclidean distance does show periodic behavior with the orbit period. The differences between Figure 9 and 11 can be attributed to the unmodeled dynamics and the spacecraft's continuous maneuvering to reject those perturbations.

The Mahalonobis distance plot, in Figure 12, also bears resemblance to the synthetic data plot in Figure 10, showing the same improved anomaly detection capability (higher Mahalonobis distance for a given SNR) at the 12- and 36-hour durations, where the out-of-plane displacement difference is greatest. The generally lower values of Mahalonobis distance at other durations are also likely due to unmodeled dynamics and the continuously thrusting behavior of the spacecraft data. Mahalonobis distance is only able to detect that a maneuver has occurred, but control distance can determine more information; for instance, the type of maneuver can be determined based on the control and trajectory from the trajectory optimization step. In contrast, control distance can both confirm maneuvers and provide the most likely combination of states, providing added data over the existing metrics.

On the surface, it may appear that the consistently lower SNR (or equivalently, track state uncertainty) required to associate UCTs would lead a prudent SSA operator to use the Mahalanobis distance metric. However, based on the control distance metric results, it is the view of the authors that such reliance on MD data association may, at particular points in the orbit or for specific durations, prematurely associate data and eliminate potentially useful association hypotheses. Said differently, the Mahalanobis distance metric may lead to missed associations. This is true namely because the Mahalanobis distance metric assumes that no maneuvers have taken place. The control metric distribution given the same information necessarily requires lower uncertainty (higher SNR) to claim that an anomaly has occurred because the assumed system may include controlled thrust.

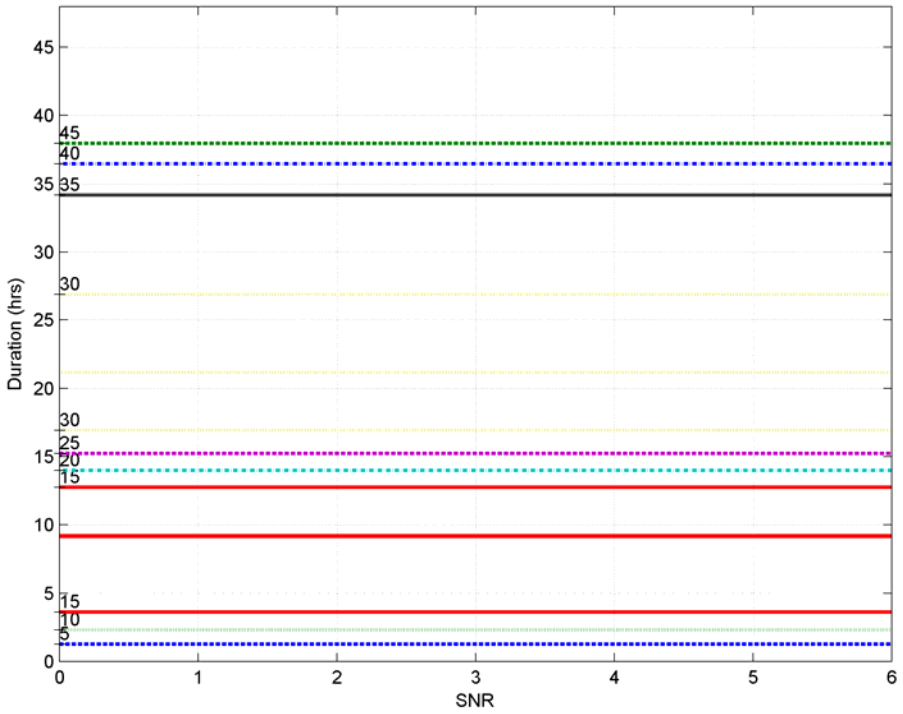

Figure 11. Euclidean Distance Metric (in km) for WAAS Scenario Sensitivity Study

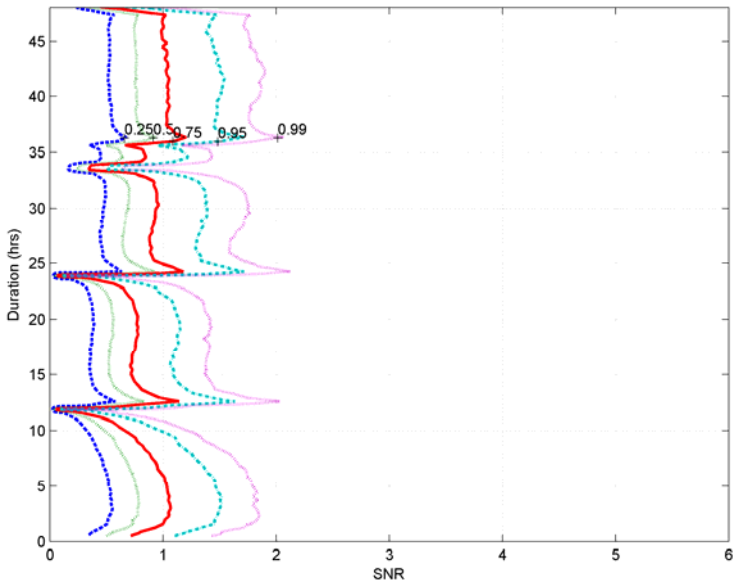

Figure 12. Mahalonobis Distance Metric for WAAS Scenario Sensitivity Study

An observation of the Mahalanobis distance computation method must be made. As previously stated, the MD implementation for this report does not model maneuvers or perturbations. One way to model such perturbations is to include process noise (dynamics uncertainty). Then, as the uncertainty covariance is propagated, the volume of the uncertainty

necessarily increases, and Mahalanobis distances for all associations naturally reduce. Thus, when process noise is included, fewer track association hypotheses are eliminated, as in the control distance results. The problem with this approach, however, is two-fold: 1) maneuvers result in structured accelerations, and are not well modeled with random accelerations assumed using process noise, and 2) to appropriately choose the process noise to capture the maneuvering trajectory, one must first know the approximate size of the maneuver, resulting in a 'chicken or the egg' problem.

To summarize, the Mahalanobis distance metric functions well as an UCT association method when space objects (SOs) are quiescent or when there are no other nearby SOs. However, if maneuvers occur, particularly when clusters of SOs are concerned, the Mahalanobis distance metric eliminates credible association hypotheses because active structured maneuvers are not considered.

5.0 CONCLUSIONS

This research demonstrates the application, effectiveness, and limitations of the DAMMM algorithm. The algorithm is designed to solve the two-point boundary value problem of space object observations to address the needs of object track correlation and maneuver characterization. The method makes use of control cost as a distance metric, constructing a trajectory to connect the boundary conditions under Keplerian dynamics and optimal control assumptions. A scenario is constructed to mirror a station-keeping maneuver, and the results were compared to actual station-keeping maneuvers from WAAS observational data of the Galaxy 15 spacecraft. Additionally, the limitations of the algorithm are tested to determine the sensitivity of the algorithm to sensor noise and observation times. In general, anomaly probability is consistent with varying duration and constant SNR. Finally, the control distance metric is compared to other common distance metrics to highlight the advantages of using control distance to correlate object tracks.

REFERENCES

1. James, L., "Keeping the Space Environment Safe for Civil and Commercial Users," *Statement of Lieutenant General Larry James, Commander, Joint Functional Component Command for Space, Before the Subcommittee on Space and Aeronautics, House Committee on Science and Technology,* April 2009.

2. "The Space Report 2011," *Space Foundation*, Colorado Springs, CO, 2011.

3. *Intelligent Data Fusion for Improved Space Situational Awareness*, Los Angeles, September 2005.

4. *Satellite Mission Operations Improvements Through Covariance Based Methods*, Laurel, MD, April 2002. AIAA-2002-1814.

5. Kelso, T. S., "Analysis of the Iridium 33 – Cosmos 2251 Collision," *Advanced Maui Optical and Space Surveillance Technologies Conference*, Maui, HI, September 2009.

6. Holzinger, M. J., "Delta-V Metrics for Object Correlation, Maneuver Detection, and Maneuver Characterization," *AIAA Guidance, Navigation, and Control Conference*, Portland, OR, August 2011.

7. Holzinger, M. J., Scheeres, D. J., and Alfriend, K. T., "Delta-V Distance Object Correlation and Maneuver Detection with Dynamics Parameter Uncertainty and Generalized Constraints," *Proceedings of the 219th American Astronomical Society Meeting*, Austin, TX, January 2012.

8. Holzinger, M. J., Scheeres, D. J., and Alfriend, K. T., "Object Correlation, Maneuver Detection, and Characterization Using Control-Distance Metrics," *Journal of Guidance, Control, and Dynamics*, **35**, 4, July 2012, pp. 1312-1325.

9. Gustafson, E. D., and Scheeres, D. J., "Optimal Timing of Control-Law Updates for Unstable Systems with Continuous Control," *Journal of Guidance, Control, and Dynamics*, **32**, 3, May 2009, pp. 878–887.

10. Abou-Moustafa, K.T., De La Torre, F., and Ferrie, F. P., "Designing a Metric for the Difference Between Gaussian Densities," *Brain, Body and Machine: Proceedings of an International Symposium on the Occasion of the 25th Anniversary of the McGill University Centre for Intelligent Machines,* **83**, 2010, pp. 57-70.

APPENDIX A: DAMMM Software Framework Code Description

This appendix describes the DAMMM software framework as shown in Figure 1 of the report. Each major component of the framework is described with the inputs required and outputs provided. A script can be written as a wrapper to handle the input tracks and tie the functions together as shown in Figure 1, tailored to the specific scenario encountered. All code is implemented in MATLAB.

Trajectory Optimization – *trajOptimizer.m*

```
%=========================================================================
%[optTraj] = trajOptimizer(scenario,settings)
%
%  Solves a two-point boundary value problem to corresponding to the input
%  scenario. Using Keplerian orbital dynamics, the optimizer seeks to find
%  the thrust accelerations required to optimally maneuver a spacecraft
%  to match the boundary conditions using a quadratic cost function,
%  consistent with variable-specific impulse engine performance. The
%  constrained minimization function (fmincon) utilizes well-known
%  gradients for the cost function and dynamics constraints to improve
%  convergence performance, and the settings structure input can be used to
%  further tune optimizer performance.
%
%INPUT
%  scenario     structure defining scenario, must contain the following
%               fields:
%                   'x0' - 6x1 vector, initial ECI state (km, km/s)
%                   'xf' - 6x1 vector, final ECI state (km, km/s)
%                   't0' - 1x1 scalar, initial time (s)
%                   'tf' - 1x1 scalar, final time (s)
%                   'dt' - 1x1 scalar, time step (s)
%  settings     structure containing settings for optimization routine,
%               contains the following fields:
%                   'maxFuncCalls' - 1x1 scalar, maximum number of steps to
%                                    use in optimization routine
%                                    default: 3000
%                   'abstol'       - 1x1 scalar, absolute convergence
%                                    tolerance in optimizer
%                   'reltol'       - 1x1 scalar, relative convergence
%                                    tolerance in optimizer
%                   'tolx'         - 1x1 scalar, termination tolerance for
%                                    changes in decision variable
%                                    default: 1e-10
%                   'tolcon'       - 1x1 scalar, tolerance on constraint
%                                    violation
%                                    default: 1e-6
%                   'genGuess'     - boolean, true to generate a guess of
%                                    control inputs to prime the optimizer
%                   'useGradients' - boolean, true to use gradients in cost
%                                    function and trajectory constraints,
%                                    default: 'true'
%                   'displayMode'  - string, selects display mode for
%                                    optimizer, review fmincon 'Display'
%                                    for options
%
```

```
%OUTPUT
%  optTraj      structure containing resulting optimal trajectory data
%                   'time'       - 1xn vector, simulation time steps (s)
%                   'trajectory' - 6xn vector, state at each time step for
%                                  optimal trajectory (km, km/s)
%                   'control'    - 3xn vector, thrust accelerations at each
%                                  time step for optimal trajectory
%                                  (km/s^2)
%                   'dV'         - 1x1 scalar, delta-v computed by
%                                  integrating thrust acceleration output
%                                  (km/s)
%                   'cost'       - 1x1 scalar, optimal quadratic control
%                                  cost (km^2/s^3)
%
%-------------------------------------------------------------------------
```

Fit Adjoints – *fitAdjoints.m*

```
%=========================================================================
%[xstar,pstar,ustar,tstar] = fitAdjoints(xInp,uInp,tInp,mu,Re)
%
% Convert the direct trajectory (x(t),u(t)) with quadratic control cost to
% an equivalent indirect trajectory (e.g., x0, p0). Uses input control
% array to generate costate guess under assumptions of optimal control,
% iteratively update costate guesses until costate guess converges.
% Propagates new indirect trajectory using Keplerian dynamics to check
% errir between new optimal trajectory and input trajectory.
%
%INPUT
%  xInp - 6xn array, direct trajectory states (km, km/s)
%  uInp - 3xn array, direct trajectory controls (km/s^2)
%  tInp - 1xn vector, direct trajectory times (s)
%  mu   - 1x1 scalar, gravitational parameter of planet
%  Re   - 1x1 scalar, equatorial radius of planet
%
%OUTPUT
%  xstar - 6xn array, optimal indirect trajectory states  (km, km/s)
%  pstar - 6xn array, optimal indirect trajectory costates
%  ustar - 3xn array, optimal indirect trajectory controls  (km/s^2)
%  tstar - 1xn vector, optimal indirect trajectory times (s)
%
%-------------------------------------------------------------------------
```

Compute Cost Distribution – *genCostDist.m*

```
%=========================================================================
%[pdf_cost,quad_cost,min_cost,mu_Pu,sig_Pu]
%                       = genCostDist(xvec,pvec,tvec,BCs,Pkk,params)
%
% Generate cost distribution for nominal indirect trajectory given boundary
% condition and systemic uncertainty inputs.
%
%INPUTS
%  xvec     6xn km, km/s, mean state space trajectory over t
%  pvec     6xn (), ()/s, mean adjoint trajectory over t
```

```
%  tvec     1xn s, time vector
%  BCs      Cell array of boundary conditions, i=1,...,Np.  Each BC has four
parameters
%   BC{i}.t 1x1 scalar time of boundary condition
%   BC{i}.P pxp covariance matrix of ith boundary condition uncertainty
%   BC{i}.y px1 nominal (mean) ith boundary condition value
%   BC{i}.H pxn partial derivative of ith boundary condition (\partial g
/partial x)
%  Pkk      2x2 covariance matrix of dynamics parameter uncertainty(ies)
%           (atmospheric density and ballistic coefficient)
%  params   Cell array of dynamics parameters parameters
%   params{1}   1x1, km^2/s^3, MU, Central body gravitational constant
%   params{2}   1x1, (), J2 coefficient
%   params{3}   1x1, (), J3 coefficient
%   params{4}   1x1, km, Radius of central body
%   params{5}   1x1, kg/m^2, Atmospheric density
%   params{6}   1x1, kg/m^2, Ballistic coefficient
%   params{7}   1x1, km/s^2, Maximum available thrust acceleration
%
%OUTPUTS
%  pdf_cost  - 1xr probability distribution of quadratic control costs
%  cost_dist - 1xr quadratic cost values for pdf_cost (km^2/s^3)
%  min_cost  - 1x1 minimum detectible quadratic cost (expectation of
%              systemic uncertainty) (km^2/s^3)
%  mu_Pu     - 1x1 first moment of cost distribution
%  sig_Pu    - 1x1 second moment of cost distribution
%
%-------------------------------------------------------------------------
```

Test Anomaly Hypothesis – *det_anomaly_cost.m*

```
%=========================================================================
%[p_anomaly,details] = det_anomaly(pdf_DV,DV,method,det_params)
%
% Determine the probability that an anomaly has occurred. Given input
% distribution  and trajectory data, determine probability that the observed
% state change is attributable to anomaly or uncertainty in state.
%
%INPUT
%  pdf_cost   - 1xr probability distribution of Delta V
%  cost_dist  - 1xr Delta V values for pdf_DV
%  method       string argument for detection method to be used.  Options
%               are 'HSA' (Holzinger-Scheeres-Alfriend)
%  det_params - cell of detection parameters for the method selected
%  mu_Pu      - 1x1 first moment of cost distribution
%  sig_Pu     - 1x1 second moment of cost distribution
%
%OUTPUT
%  p_anomaly - 1x1 probability that an anomaly has occured
%  details   - method dependent structure of ancillary information
%
%-------------------------------------------------------------------------
```

APPENDIX B: Theory Extension

This appendix describes novel theoretical results that may be used to compute the distribution of quadratic control distances using Gaussian mixtures as boundary condition uncertainties.

The quadratic control cost for a single term of the Gaussian sum connecting Gaussian initial distribution *I* to Gaussian final distribution *j* may be described as

$$P_{ij} = l_{ij} + \boldsymbol{m}_{ij}^T \boldsymbol{V}_{ij} + \boldsymbol{V}_{ij} \boldsymbol{N}_{ij} \boldsymbol{V}_{ij} \tag{B-1}$$

where $l_{ij} \in \mathbb{R}$, $\boldsymbol{m}_{ij}^T \in \mathbb{R}^{2n}$, $\boldsymbol{N}_{ij} \in \mathbb{R}^{2n \times 2n}$, and the random variable $\boldsymbol{V} \sim N(\boldsymbol{\mu}_{ij}, \boldsymbol{P}_{V,ij})$, where $\mathrm{E}[\boldsymbol{V}_{ij}] = \boldsymbol{\mu}_{ij}$ and $\mathrm{E}\left[\mathrm{E}[\boldsymbol{V}_{ij}]^T \mathrm{E}[\boldsymbol{V}_{ij}] - \mathrm{E}[\boldsymbol{V}_{ij} \boldsymbol{V}_{ij}^T]\right] = \boldsymbol{P}_{V,ij}$. Defining a new random variable $\boldsymbol{W}_{ij}$ such that

$$\boldsymbol{W}_{ij} = \boldsymbol{V}_{ij} - \boldsymbol{\mu}_{ij}$$

where now $\boldsymbol{W} \sim N(\boldsymbol{0}, \boldsymbol{P}_{V,ij})$. The cost P_{ij} can be re-written in terms of this new random variable using direct substitution:

$$\begin{aligned} P_{ij} &= l_{ij} + \boldsymbol{m}_{ij}^T (\boldsymbol{\mu}_{ij} + \boldsymbol{W}_{ij}) + (\boldsymbol{\mu}_{ij} + \boldsymbol{W}_{ij})^T \boldsymbol{N}_{ij} (\boldsymbol{\mu}_{ij} + \boldsymbol{W}_{ij}) \\ &= l_{ij} + \boldsymbol{m}_{ij}^T \boldsymbol{\mu}_{ij} + \boldsymbol{m}_{ij}^T \boldsymbol{W}_{ij} + \boldsymbol{\mu}_{ij}^T \boldsymbol{N}_{ij} \boldsymbol{\mu}_{ij} + 2\boldsymbol{\mu}_{ij}^T \boldsymbol{N}_{ij} \boldsymbol{W}_{ij} + \boldsymbol{W}_{ij}^T \boldsymbol{N}_{ij} \boldsymbol{W}_{ij} \\ &= (l_{ij} + \boldsymbol{m}_{ij}^T \boldsymbol{\mu}_{ij} + \boldsymbol{\mu}_{ij}^T \boldsymbol{N}_{ij} \boldsymbol{\mu}_{ij}) + (\boldsymbol{m}_{ij}^T + 2\boldsymbol{\mu}_{ij}^T \boldsymbol{N}_{ij}) \boldsymbol{W}_{ij} + \boldsymbol{W}_{ij}^T \boldsymbol{N}_{ij} \boldsymbol{W}_{ij} \end{aligned}$$

If the following definitions are made:

$$\begin{aligned} \tilde{l}_{ij} &= l_{ij} + \boldsymbol{m}_{ij}^T \boldsymbol{\mu}_{ij} + \boldsymbol{\mu}_{ij}^T \boldsymbol{N}_{ij} \boldsymbol{\mu}_{ij} \\ \widetilde{\boldsymbol{m}}_{ij} &= \boldsymbol{m}_{ij}^T + 2\boldsymbol{\mu}_{ij}^T \boldsymbol{N}_{ij} \end{aligned}$$

then Equation B-1 may be rewritten in a nearly identical form using the zero-mean random variable $\boldsymbol{W}_{ij}$ as

$$P_{ij} = \tilde{l}_{ij} + \widetilde{\boldsymbol{m}}_{ij}^T \boldsymbol{W}_{ij} + \boldsymbol{W}_{ij}^T \boldsymbol{N}_{ij} \boldsymbol{W}_{ij} \tag{B-2}$$

From Holzinger et al. (see reference 8), Appendix B, the analytic first and second moments of P_{ij} may be written as:

$$\begin{aligned} \mathrm{E}[P_{ij}] &= \boldsymbol{\mu}_{P,ij} = l_{ij} + \boldsymbol{m}_{ij}^T \boldsymbol{\mu}_{ij} + \boldsymbol{\mu}_{ij}^T \boldsymbol{N}_{ij} \boldsymbol{\mu}_{ij} + \mathrm{Tr}[\boldsymbol{N}_{ij} \boldsymbol{P}_{V,ij}] \\ \mathrm{E}[P_{ij}^2] &= \sigma_{P,ij}^2 = (\boldsymbol{m}_{ij}^T + 2\boldsymbol{\mu}_{ij}^T \boldsymbol{N}_{ij})^T \boldsymbol{P}_{V,ij} (\boldsymbol{m}_{ij}^T + 2\boldsymbol{\mu}_{ij}^T \boldsymbol{N}_{ij}) + 2\mathrm{Tr}[\boldsymbol{N}_{ij} \boldsymbol{P}_{V,ij} \boldsymbol{N}_{ij} \boldsymbol{P}_{V,ij}] \end{aligned}$$

The total cost of all *i* initial boundary conditions and *j* final boundary conditions is the weighted sum of the individual costs between each *i* and *j*:

$$P = \sum_i \sum_j w_i w_j P_{ij}$$

where w_i is the weight of the i^{th} initial boundary condition and w_j is the weight of the j^{th} final boundary condition. Thus, the analytic expected value of the initial and final Gaussian sum boundary conditions may be written as:

$$\begin{aligned} \mathrm{E}[P] &= \mathrm{E}\left[\sum_i \sum_j w_i w_j P_{ij}\right] \\ &= \sum_i \sum_j w_i w_j \mathrm{E}\left[P_{ij}\right] \\ &= \sum_i \sum_j w_i w_j \boldsymbol{\mu}_{ij} \end{aligned}$$

which leads to the final result:

$$\boldsymbol{\mu}_P = \textstyle\sum_i \sum_j w_i w_j \left(l_{ij} + \boldsymbol{m}_{ij}^T \boldsymbol{\mu}_{ij} + \boldsymbol{\mu}_{ij}^T \boldsymbol{N}_{ij} \boldsymbol{\mu}_{ij} + \mathrm{Tr}\left[\boldsymbol{N}_{ij} \boldsymbol{P}_{V,ij}\right]\right) \qquad \text{(B-3)}$$

LIST OF SYMBOLS, ABBREVIATIONS, AND ACRONYMS

AFRL	Air Force Research Laboratory
CDF	Cumulative distribution function
DAMMM	Data association using a minimum-fuel maneuver metric
ECEF	Earth-centered Earth-fixed
GEO	Geostationary Earth orbit
MD	Mahalonobis Distance
PDF	Probability density function
PI	Principal investigator
RIC	Radial, in-track, and cross-track
RAM	Random access memory
RSO	Resident space object
SNR	Signal-to-noise ratio
SO	Space object
SSA	Space situational awareness
SoW	Statement of work
TPBVP	Two-point Boundary Value Problem
UCT	Uncorrelated track
VSI	Variable specific impulse engines
WAAS	Wide Area Augmentation System

DISTRIBUTION LIST

DTIC/OCP
8725 John J. Kingman Rd, Suite 0944
Ft Belvoir, VA 22060-6218 1 cy

AFRL/RVIL
Kirtland AFB, NM 87117-5776 2 cys

Official Record Copy
AFRL/RVSV/Morgan Baldwin 1 cy

(This page intentionally left blank)